Hydrogenation of CO_2 and CO in a High Temperature Gradient Field between Catalyst Surface and Opposite Inert Cool Plate

David Perko and Andrej Pohar
Laboratory of Catalysis and Chemical Reaction Engineering, National Institute of Chemistry, 1000 Ljubljana, Slovenia

Janez Levec
Laboratory of Catalysis and Chemical Reaction Engineering, National Institute of Chemistry and Faculty of Chemistry and Chemical Technology, University of Ljubljana, 1000 Ljubljana, Slovenia

DOI 10.1002/aic.14280
Published online November 15, 2013 in Wiley Online Library (wileyonlinelibrary.com)

Methanol synthesis was carried out at 25 bar in slit formed by two parallel plates 5 mm apart. Upper plate was covered by catalyst layer and heated up to 250°C, whereas lower one was kept at about 30°C. Reaction stream in laminar flow consisted of H_2, CO_2, and CO in concentration range usually encountered in industrial processes. Catalyst layer was prepared by spraying $CuO/ZnO/Al_2O_3/V_2O_3$ slurry on SS-plate. Continuous removal of methanol and water by condensation on the cool surface shifted equilibrium toward products formation. At isothermal conditions with no temperature gradient in slit, total carbon conversion approached the thermodynamic equilibrium when residence time was long enough. Experiments with high temperature difference showed total carbon conversion much larger compared to the thermodynamic one calculated at plate-catalyst temperature. Three-dimensional model predicted total carbon conversion for both isothermal and high temperature gradient operation reasonably well. © 2013 American Institute of Chemical Engineers *AIChE J*, 60: 613–622, 2014

Keywords: methanol synthesis, reaction kinetics, process intensification, multifunctional reactor, mathematical modeling

Introduction

It is of fundamental as well as practical interest to know what level of conversion beyond the equilibrium one can be accomplished if an exothermic reversible catalytic reaction is taking place in a slit formed by two parallel plates, where one is covered with an active catalyst and maintained at high temperature, while the opposite one, where the products condense, is catalytically inert and kept at low temperature. Thus, the question is what increase of the production rate can be expected in the case the reaction is carried out in a gap of high temperature gradient (HTG), which consequently generates high gradients in the products partial pressures and thus drive them away from the catalyst surface. A shift of the global equilibrium may be called the thermodynamic pump. In a way, employment of the thermodynamic pump principle to shift the equilibrium was first reported by Halloin and Wajc,[1] and Amor and Halloin,[2] who used an annular type fixed bed reactor for methanol synthesis. In their study, the gaseous reactants and products passed the bed radially and less volatile products (methanol and water) condensed on the outer cooled wall, which enveloped the catalyst bed. The gas-phase was kept inside the reactor, thus only the condensed products (mainly methanol) could leave the reactor. Consequently, they claimed increased conversions in comparison to the conventional process, which was caused by several orders of magnitude higher space times. By inspecting their experimental device more in detail, one can conclude that it had characteristics similar to a standard fixed bed with an internal condenser.[3] It was recently demonstrated that the condensation of reaction products drives the equilibrium reactions nearly to completion.[4]

In order to provide the proof of concept for the thermodynamic pump one needs an experimental device that could offer the temperature gradient mentioned earlier. For that purpose, it is also necessary to prepare a durable and stable catalytically active layer on a metal substrate (plate-type catalyst). Reactors with plate-type catalysts are known to have some advantageous properties in high exothermic or endothermic reaction systems. This type of catalyst has been successfully demonstrated in microstructured reactors for methanol reforming[5–7] and methanol synthesis.[8] Due to a very thin catalyst layer (in the order of 100 μm) plate-type catalysts operate isothermally and do not exhibit intraparticle diffusion resistance, which is an important issue for high reaction rate systems. The most frequently used technique to make a wall coating of catalyst slurries on nonporous microchannel walls is the so-called gas-assisted fluid displacement method or washcoating,[9] while foil coating was efficiently demonstrated by a sol-gel and impregnation technique.[8]

The aim of this work was to demonstrate the efficiency of a thermodynamic pump with methanol synthesis carried out in a narrow slit with a high transverse temperature gradient

Correspondence concerning this article should be addressed to J. Levec at janez.levec@ki.si.

(HTG mode) between the plate-type catalyst and opposite inert cool surface—in the order of 200°C over a distance of few millimeters. The gas-phase flow in the slit was laminar. A simple spraying technique for catalyst slurry deposition on a stainless steel (SS) substrate was used for making a durable plate-type catalyst.[10] A mathematical model, which accounts for the intrinsic rate of CO and CO_2 hydrogenation, as well as the water-gas-shift reaction, was developed in order to compare the predicted and experimental results obtained with and without the transverse temperature gradient (i.e., isothermal operation, IT mode).

Experimental

Reactor with plate-catalyst

A schematic drawing of the reactor system used in this study is depicted in Figure 1. Details are found elsewhere.[11] The reactor consisted of two parts: an upper and a lower SS-304 horizontal block with dimensions of 600 × 280 × 80 mm and 600 × 280 × 40 mm, respectively. In the upper block, a heat exchanger with the plate-catalyst was incorporated but isolated from the metal block in order to minimize heat loss (Figures 1, 2). The SS plate on which the catalyst layer was deposited had the dimensions of 260 × 140 × 7 mm, whereas the catalyst layer covered only the area of 240 × 120 mm. The exchanger was heated by oil passing through machined grooves (cross section 6 × 7 mm), which were systematically distributed (four independent streams of oil in a groove of 0.85 m in length) over the whole plate. With this heating arrangement it was possible to maintain uniform temperature over the whole area of the catalyst layer (240 × 120 mm) within ±2°C at temperatures up to 250°C (Figure 3a).

The lower block consisted of an engraved niche as shown in Figure 4 with dimensions 330 × 169 × 10 mm. At the bottom of the niche there was an aluminum plate (330 × 164 × 5 mm) so that the distance between the plate-catalyst and aluminum plate was 5 mm. The effective volume of the niche, which in fact represented the reactor volume, was about 300 cm^3. The aluminum plate consisted of a series of

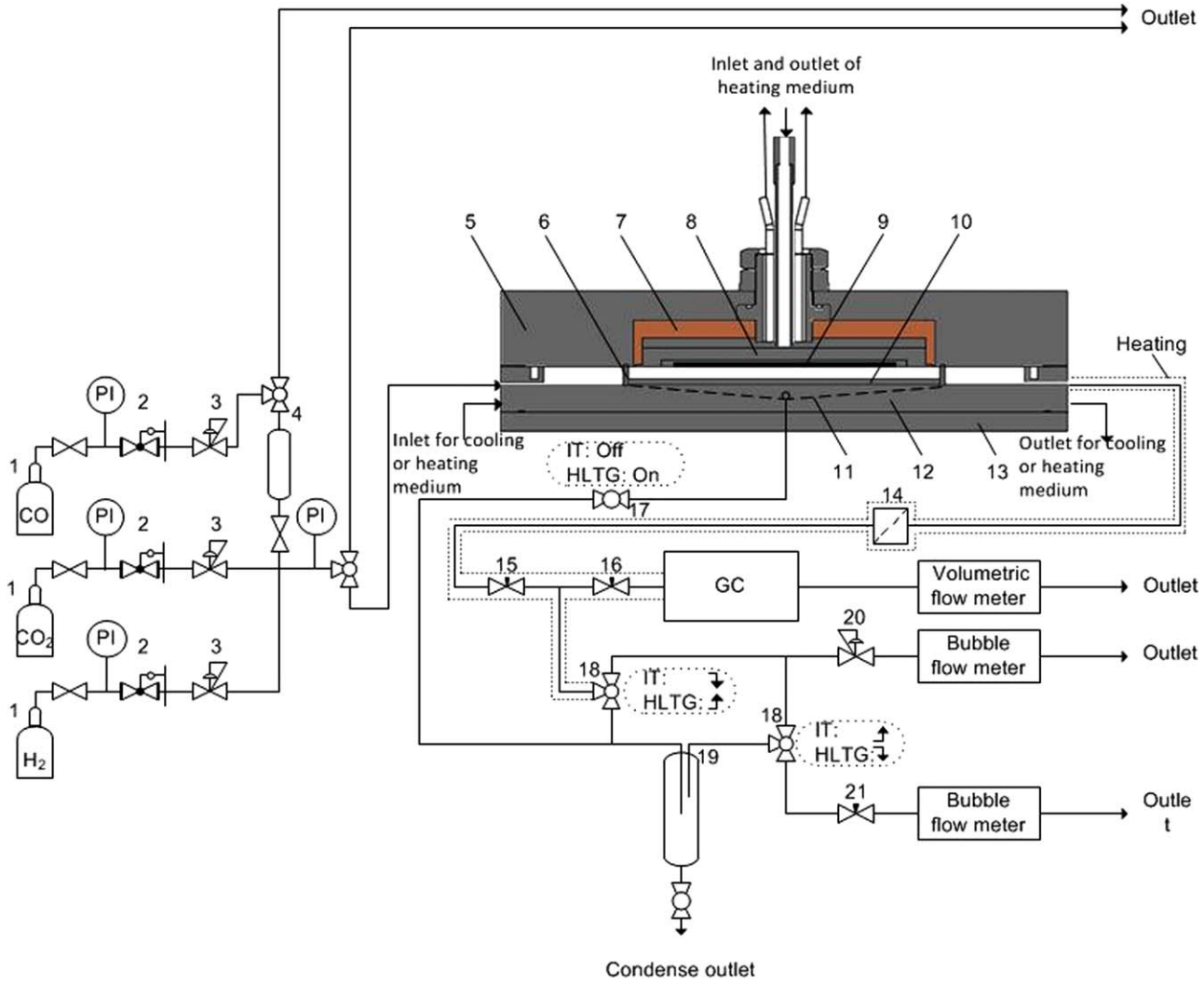

Figure 1. Scheme of the experimental setup: (1) gas cylinders, (2) pressure reducers, (3) mass flow controllers, (4) molecular sieves 13X, (5) upper metal block, (6) gas distributor, (7) thermal isolation, (8) heat exchanger, (9) catalytic layer, (10) lower horizontal plate, (11) side drainage channel, (12) lower metal block, (13) cover for lower metal block, (14) filter, (15) needle valve, (16) fine needle valve, (17) ball valve, (18) three way ball valve, (19) gas-liquid separator, (20) back pressure regulator, (21) needle valve.

[Color figure can be viewed in the online issue, which is available at wileyonlinelibrary.com.]

Figure 2. Heat exchanger with plate-catalyst incorporated into upper metal block.

Picture taken after experiments. [Color figure can be viewed in the online issue, which is available at wileyonlinelibrary.com.]

miniature capillary grooves (0.5 × 0.5 mm) for collecting the condensable products, that is, methanol and water. The grooves acted as capillaries and efficiently drained off the liquid condensate; in that way water was not accumulated on the plate area during the experiments. The condensate was continuously removed through small channels at the edge of the plate. To push the condensate out of the reactor, a small portion of the gas stream was necessary to accompany the liquid (about 0.8 mol. % of the gas phase fed into the reactor). However, the performance of the aluminum plate was verified in cold operation. The lower block was efficiently cooled (HTG mode) by a stream of tap water through two channels (cross section 10 × 10 mm) of 1.5 m in length distributed in an efficient pattern (Figure 3b), so that the surface temperature of the lower aluminum plate was kept constant slightly above room temperature (32 ± 2°C). It was assumed that the temperature gradient between 200 and 230°C established in the reactor was high enough for checking the thermodynamic pump concept. In the case of operation in the IT mode, the lower block was heated by the same source of oil as was used for the upper heat exchanger.

The gas-phase entered and left the reactor space through an array of small holes (dia. 0.4 mm) in the aluminum crossbars, which spanned the niche cross-section and acted as a

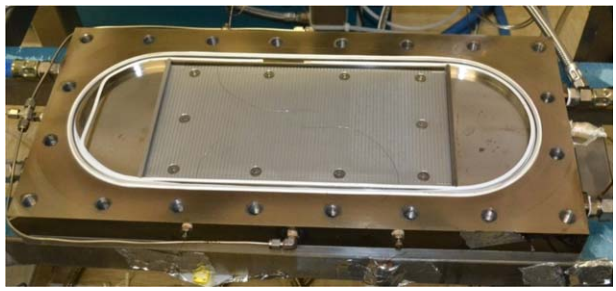

Figure 4. Lower metal block with aluminum plate and gas distributors.

[Color figure can be viewed in the online issue, which is available at wileyonlinelibrary.com.]

gas distributor. The distance from the crossbar to the catalyst layer was 4.5 cm. The calculations showed that at the conditions used, the parabolic flow profile was fully developed already after 7–8 mm. In the IT mode, the reactor was insulated at the nonheated outer surfaces to minimize heat loss from the reactor, thus facilitating isothermal operation. The temperature on the surface of the plate-catalyst as well as the temperature on the aluminum plate surface was measured with 0.25 mm K-type thermocouples (KMQSS-010U-12; Omega Engineering) placed in direct contact with the surfaces. The reactor temperature was controlled by means of an oil-thermostat (TEMP 300, Boe-Therm), whereas the reactor pressure was controlled by a back pressure controller (26–1723, Tescom).

The reactants H_2 (purity 5.0–Messer), CO (purity 3.7–Linde), and CO_2 (purity 4.8–Messer) were fed into the reactor through a set of mass flow controllers (Brooks 5850TR and 5850S). The experiments were mainly performed with two gas-reactant mixtures (mol. % of H_2/CO/CO_2): 0.71/0.19/0.10 and 0.78/0.12/0.10, respectively. The formation of nickel tetracarbonyl and iron pentacarbonyl likely happens when CO comes into contact with materials containing Ni and Fe (in SS) at 50–150°C.[12] To prevent possible catalyst deactivation due to nickel tetracarbonyl and iron pentacarbonyl decomposition at the temperatures used for methanol synthesis, a column packed with 13X molecular sieves was placed behind the CO feeding mass flow controller. Copper tubes were used in the part of the feed section where CO was present.

Figure 3. Grooved channels in (a) heat exchanger and (b) lower metal block.

[Color figure can be viewed in the online issue, which is available at wileyonlinelibrary.com.]

Preparation of plate-catalyst

A detailed method for preparing plate-type catalysts is described elsewhere.[10] A proprietary methanol synthesis catalyst $CuO/ZnO/Al_2O_3/V_2O_3$ (Lurgi GmbH; 59/32/4/5 wt. %) in the form of tablets was first milled in a ball mill after which the powder was suspended in 2-propanol to form a 10 wt. % suspension, which was sprayed with an airbrush on a heated SS 304 plate with dimensions 240 × 120 mm. The catalyst coating was estimated to have a thickness of 95 ± 10 μm, thus the total mass of catalyst was about 4.7 g. X-ray diffraction, energy-dispersive X-ray spectroscopy, and total carbon analysis were applied on the catalyst coating before and after exposing it to the reaction conditions. The mass loss of the catalyst coating during the experiments was found to be insignificant, which alludes to excellent layer adherence. Figure 2 shows the catalyst coating after 22 days on stream at the reaction conditions. The IT experiments were carried out first, after which the HTG experiments were executed. Catalyst deactivation was assumed to be the same as evaluated in a previous work.[10] According to the findings of Bussche and Froment,[13] who showed the absence of diffusional resistance within particles bellow 700 μm in diameter and higher temperatures than those used in this study, the intralayer diffusional limitations were considered negligible.

Analysis

Analyses of the gaseous streams coming in and out of the reactor were carried out with a gas chromatograph (7890A, Agilent Technologies) equipped with TCD detectors and HAYESEP Q, HP-PLOT Q, MOLESIEVE 5A columns (Agilent Technologies). He and N_2 were used as carrier gases. To observe the steady-state operation, concentrations of CO and CO_2 in the exit stream was monitored by a nondispersive IR detector (Binos 1001, Rosemount). The total carbon conversion of the gas reaction mixture (CO_2 and CO only) was calculated according to the relation

$$X_c = \frac{(\dot{n}_{CO} + \dot{n}_{CO_2})_{in} - (\dot{n}_{CO} + \dot{n}_{CO_2})_{out}}{(\dot{n}_{CO} + \dot{n}_{CO_2})_{in}} \quad (1)$$

where $(\dot{n}_{CO} + \dot{n}_{CO_2})_{in}$ and $(\dot{n}_{CO} + \dot{n}_{CO_2})_{out}$ represent the molar flow rates of CO and CO_2 in/out of the system. In the IT as well as in the HTG mode, the inlet molar flow rates of CO and CO_2, that is, $(\dot{n}_{CO} + \dot{n}_{CO_2})_{in}$, were adjusted by mass flow controllers. In the IT mode, the outlet molar flow rates of CO and CO_2 were obtained with

$$(\dot{n}_{CO} + \dot{n}_{CO_2})_{out} = \frac{\dot{m}_{out}}{M_{out}} (x_{CO} + x_{CO_2})_{out} \quad (2)$$

where $\dot{m}_{out}$ is the total mass flow rate of the gas phase from the reactor and M_{out} the outlet average molar mass.

In the HTG mode of operation, CO and CO_2 left the reactor at four different outlets (see Figure 5) therefore the total outlet carbon molar flow rate was calculated accordingly

$$(\dot{n}_{CO} + \dot{n}_{CO_2})_{out} = \sum_{i=1}^{4} (\dot{n}_{CO} + \dot{n}_{CO_2})_{out,i} \quad (3)$$

At the points where the gas-phase left the system ($i = 1$, 2, 3) the individual carbon molar flow rates were obtained on the basis of the measured volumetric flow rates and the gas compositions, thus

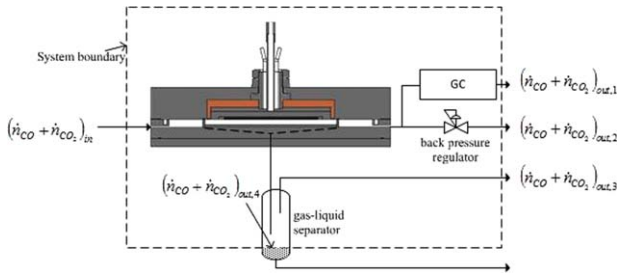

Figure 5. CO and CO_2 flow in HTG mode operation.

[Color figure can be viewed in the online issue, which is available at wileyonlinelibrary.com.]

$$(\dot{n}_{CO} + \dot{n}_{CO_2})_{out,i} = \left(\frac{Q_v p}{RT} (x_{CO} + x_{CO_2})\right)_{out,i} \quad (4)$$

where Q_v is the volumetric flow rate, p is the pressure, R is the gas constant, and T is the temperature.

Since the flow rate of the gas-phase leaving the gas-liquid separator was very low, the carbon mole fraction in that stream, that is, $(x_{CO} + x_{CO_2})_{out,3}$, was estimated as an average value between $(x_{CO} + x_{CO_2})_{in}$ and $(x_{CO} + x_{CO_2})_{out,2}$.

The solubility of CO and CO_2 in the condensate (mixture of methanol and water) was also considered and their molar flow rates were estimated by

$$(\dot{n}_{CO} + \dot{n}_{CO_2})_{out,4} = \left(\frac{\dot{m}_{con}}{M_{con}} (x_{CO} + x_{CO_2})\right)_{out,4} \quad (5)$$

where M_{con} denotes average condensate molar mass and $\dot{m}_{con}$ total mass flow rate of the liquid phase leaving the system. The molar fractions of CO and CO_2 in the liquid phase were estimated by Henry's law

$$(x_{CO} + x_{CO_2})_{out,4} = \frac{p_{CO}}{H_{mix,CO}} + \frac{p_{CO_2}}{H_{mix,CO_2}} \quad (6)$$

The Henry's constants ($H_{mix,j}$) for components CO or CO_2 in the binary mixture of methanol and water were estimated by the relation of Shulgin and Ruckenstein.[14] The calculations showed very low solubility of CO and CO_2 in the condensate, that is, less than 1.3 mol. % at the conditions used.

Model Formulation

To shed some light on the processes in the slit with the HTG, a 3-D model was formulated. It was based on the following geometrical facts: the slit height 5 mm (z-coordinate), the length 240 mm (y-coordinate), whereas its lateral dimension (x-coordinate) was 169 mm, that is, the lateral width-to-height ratio was 34 (see schematics of the slit in Figure 6). Due to low Reynolds numbers (below 8) one may assume laminar flow of the gas phase in the slit.

It was further assumed:

- the gas phase is considered as a Newtonian, compressible fluid,
- in the catalyst layer there is no mass/heat transfer limitation, reactions on the surface enter into the model as boundary conditions,
- methanol and water condense in the form of a film, which is infinitively thin and there is no mist present,
- partial pressures of methanol and water in the gas phase at the gas-liquid film boundary correlate to those in the liquid film by Raoult's law,

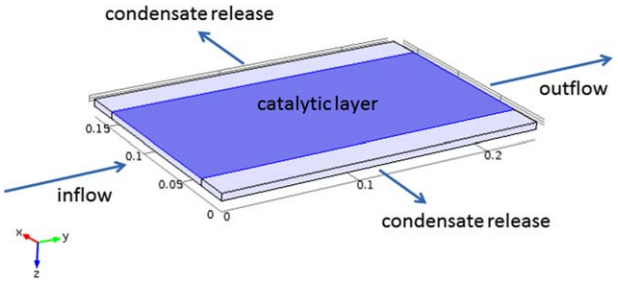

Figure 6. Geometrical domain of slit with catalyst layer.

[Color figure can be viewed in the online issue, which is available at wileyonlinelibrary.com.]

- solubility of H_2, CO, and CO_2 in the condensate is neglected,
- heat transport by diffusing species and radiation, viscous dissipation, as well as the Dufour effect are assumed unimportant and not accounted for in the energy balance,
- in the species mass balances, the contribution of thermal diffusion is also disregarded.

The above assumptions simplify the reactor model and enable fast computation and comparison of the predicted results with the experimental ones. A steady-state three-dimensional model without adjustable parameters is thus governed by the following equations: the continuity equation

$$\nabla(\rho\mathbf{u})=0 \tag{7}$$

where ρ is the gas density and $\mathbf{u}$ is the velocity vector. The momentum equation is given in the form

$$\rho\mathbf{u}\cdot\nabla\mathbf{u}=-\nabla p+\nabla\cdot\left(\mu\left(\nabla\mathbf{u}+(\nabla\mathbf{u})^T\right)\right)+\nabla\cdot\left(-\frac{2\mu}{3}\nabla\cdot\mathbf{u}\right) \tag{8}$$

where the gravitational forces are not accounted for. The energy balance is written as

$$\rho\hat{C}_p\mathbf{u}\cdot\nabla\mathrm{T}=\nabla\cdot(\lambda\nabla T) \tag{9}$$

where $\hat{C}_p$ is the heat capacity and λ is the thermal conductivity.

The species mass balance equation is written in the following form

$$\rho u\frac{\partial}{\partial x}\omega_j+\rho v\frac{\partial}{\partial y}\omega_j+\rho w\frac{\partial}{\partial z}\omega_j=\nabla\cdot\left(\rho\omega_j\sum_{k=1}^{N}\tilde{D}_{jk}\mathbf{d}_k\right) \tag{10}$$

$$j=1,2,3,...,N-1$$

$$\mathbf{d}_k=\nabla x_k+\frac{1}{p}\left[(x_k-\omega_k)\nabla p\right] \tag{11}$$

$$\omega_N=1-\sum_{j=1}^{N-1}\omega_j \tag{12}$$

$$\nabla=\vec{i}\frac{\partial}{\partial x}+\vec{j}\frac{\partial}{\partial y}+\vec{k}\frac{\partial}{\partial z} \tag{13}$$

where N represents the total number of components ($N=5$), that is, CO, CO_2, H_2O, CH_3OH, H_2, ω_j mass fraction of j-component, x_k mol fraction of k-component, $\tilde{D}_{jk}$ multicomponent Fick diffusivities, and $\mathbf{d}_k$ diffusion driving force for k-component.[15] Equation 10 was solved for $(N-1)$ components, while the mass fraction of N-component, that is, for H_2, was obtained from Eq. 12.

The earlier equations are subjected to the following boundary conditions that apply at the reactor inlet: ($y=0,\quad 0\le x\le W,\quad 0\le z\le H$)

$$\begin{aligned}
&u=u_{\mathrm{in}}, \qquad u_{\mathrm{in}}=\frac{Q_v}{A_{pp}}\\
&v=0\\
&w=0\\
&j_{x,j}|_{y=0^+}=u\rho\omega_j|_{y=0^-}-u\rho\omega_j|_{y=0^+}\\
&-\lambda\frac{dT}{dy}\bigg|_{y=0^+}=\rho\hat{C}_puT|_{y=0^-}-\rho\hat{C}_puT|_{y=0^+}
\end{aligned} \tag{14}$$

and at the reactor outlet

$$\begin{aligned}
&p=p_{\mathrm{out}}, \quad \text{no viscous stress}\\
&\frac{\partial T}{\partial y}=0\\
&j_{y,j}=0, \qquad j=1,2,3,...,N-1
\end{aligned} \tag{15}$$

The boundary conditions at the upper plate ($0\le y\le L,\ W_1\le x\le W_2,\ z=H$) are specified by the diffusional fluxes of species, which are caused by the reactions on the catalyst surface, thus

$$\begin{aligned}
&u=0\\
&v=0\\
&w=0\\
&T=T_{\mathrm{cat}}\\
&-j_{z,j}=\sum_i\left(\frac{m_{\mathrm{cat}}}{S_{\mathrm{cat}}}\alpha\nu_{j,i}r_iM_j\right), \qquad j=1,2,3,...,N-1
\end{aligned} \tag{16}$$

where r_i stands for the reaction rate of i-th reaction, $\nu_{j,i}$ for the stoichiometric coefficient of component j in i-th reaction, m_{cat} for the total mass of catalyst (i.e., 47 g), S_{cat} for the geometric surface area of the plate-catalyst (i.e., 240 × 120 mm), and α is the catalyst deactivation coefficient. W_1 in W_2 had the following values: 24.5 and 144.5 mm, respectively. The kinetics of all three reactions, hydrogenation of CO_2 ($i=3$) and CO ($i=1$), and water-gas-shift reaction ($i=2$) were studied on the plate-catalyst as described elsewhere.[10] The resulting kinetic expressions were best described by the equation type[16]

$$r_1=\frac{k'_{\mathrm{ps},1}K_{\mathrm{CO}}\left[p_{\mathrm{CO}}p_{\mathrm{H_2}}^{3/2}-p_{\mathrm{CH_3OH}}/\left(p_{\mathrm{H_2}}^{1/2}K^0_{\mathrm{p},1}\right)\right]}{\left(1+K_{\mathrm{CO}}p_{\mathrm{CO}}+K_{\mathrm{CO_2}}p_{\mathrm{CO_2}}\right)\left[p_{\mathrm{H_2}}^{1/2}+\left(K_{\mathrm{H_2O}}/K_{\mathrm{H_2}}^{1/2}\right)p_{\mathrm{H_2O}}\right]} \tag{17}$$

$$r_2=\frac{k'_{\mathrm{ps},2}K_{\mathrm{CO_2}}\left(p_{\mathrm{CO_2}}p_{\mathrm{H_2}}-p_{\mathrm{H_2O}}p_{\mathrm{CO}}/K^0_{\mathrm{p},2}\right)}{\left(1+K_{\mathrm{CO}}p_{\mathrm{CO}}+K_{\mathrm{CO_2}}p_{\mathrm{CO_2}}\right)\left[p_{\mathrm{H_2}}^{1/2}+\left(K_{\mathrm{H_2O}}/K_{\mathrm{H_2}}^{1/2}\right)p_{\mathrm{H_2O}}\right]} \tag{18}$$

$$r_3=\frac{k'_{\mathrm{ps},3}K_{\mathrm{CO_2}}\left[p_{\mathrm{CO_2}}p_{\mathrm{H_2}}^{3/2}-p_{\mathrm{CH_3OH}}p_{\mathrm{H_2O}}/\left(p_{\mathrm{H_2}}^{3/2}K^0_{\mathrm{p},3}\right)\right]}{\left(1+K_{\mathrm{CO}}p_{\mathrm{CO}}+K_{\mathrm{CO_2}}p_{\mathrm{CO_2}}\right)\left[p_{\mathrm{H_2}}^{1/2}+\left(K_{\mathrm{H_2O}}/K_{\mathrm{H_2}}^{1/2}\right)p_{\mathrm{H_2O}}\right]} \tag{19}$$

The boundary conditions at the bottom plate depend on the mode of reactor operation, that is, IT mode or the HTG mode. In the first case, the conditions are straightforward as follows

$$\begin{aligned} u&=0\\ v&=0\\ w&=0\\ T&=T_{\text{in}}=T_{\text{cat}}\\ j_{z,j}&=0 \end{aligned} \tag{20}$$

whereas in the HTG operation, the conditions must account for the fact that the temperature/concentration gradients drive the mass flux of methanol and water toward the cool condensation plate. Thus, the conditions which apply at the bottom plate are[11]

$$\begin{aligned} u&=0\\ w&=0\\ v&=\frac{j_{z,\text{CH}_3\text{OH}}+j_{z,\text{H}_2\text{O}}}{(1-(\omega_{\text{CH}_3\text{OH}}+\omega_{\text{H}_2\text{O}}))\rho}\\ T&=T_{\text{cool}}\\ \rho\omega_{\text{CO}}v+j_{z,\text{CO}}&=0\\ \rho\omega_{\text{CO}_2}v+j_{z,\text{CO}_2}&=0\\ \omega_{\text{CH}_3\text{OH}}&=\frac{x_{\text{liq,CH}_3\text{OH}}p_{\text{eq,CH}_3\text{OH}}M_{\text{CH}_3\text{OH}}}{pM}\\ \omega_{H_2O}&=\frac{x_{\text{liq,H}_2\text{O}}p_{\text{eq,H}_2\text{O}}M_{\text{H}_2\text{O}}}{pM} \end{aligned} \tag{21}$$

The condensation of water and methanol on the cool plate generated a small convection mass flux out of the geometric domain (gas phase). H_2 (N-component) was assumed to be insoluble in the condensate and thus the total mass flux of H_2 was equal to zero. Since CO_2 and CO were also assumed to be insoluble in the condensate, the total mass fluxes for both these components were also zero. The mass fraction (ω_j) of methanol and water in the gas phase above the condensate was in equilibrium with its values in the liquid film (Raoult's law). The boundary condition (21) was used for the entire length of the cool plate but for a few millimeters at the entrance, where the partial pressures of methanol and water were too low for the condensation to occur.

Model solving

The model governing equations were solved numerically with commercial finite element analysis software COMSOL Multiphysics 4.2a. The relative tolerance (of the stationary solver) was set to 10^{-4}. Several grid sizes were tested to ensure that the results were grid insensitive. The final results were obtained on a grid with 42,350 hexahedral elements (55 in x-direction, 77 in y-direction, and 10 in z-direction). The possible existence of multiple solution branches was tested by specifying different sets of initial mass fraction values for the calculation. The same unique solution was obtained in all cases, except in some cases when unreasonable starting values were chosen and the model did not converge after 80 iterations.

Results and Discussion

The plate-catalyst activity decrease was monitored by following the reduction in the total carbon conversion as a function of time-on-stream. Thus, in all IT mode experiments the total carbon conversion dropped for about 21% in a period of 78 h, whereas in the HTG experiments (which followed the IT ones); the activity was further decreased for about 20% in 210 h of continuous operation. The mechanical deactivation is positively not a reason for activity reduction since the mass loss of catalyst in the layer was found negligible after the experiments. The rate and reasons for catalyst deactivation is discussed in a paper of Perko and Levec.[10] The catalyst deactivation coefficient α was evaluated by linear interpolation between two reference rate data points. Although the reaction system possesses the characteristics, which may exhibit a sustained instability, no oscillations in the temperature (on the catalyst layer) or/and concentrations at the reactor exit were observed.

The selectivity (to methanol) of modern Cu-based catalysts is extremely high, normally above 99%.[17] GC analysis of the gaseous phase leaving the reactor showed that a very small amount of side products were formed, thus the hydrogenation of CO and CO_2 were the main carbon consuming reactions, which led to methanol formation. The carbon mass balance was usually closed within 2%. Therefore, the total carbon conversion accounted for the fraction of inlet molar flow of CO and CO_2 that was converted mainly into methanol during the passage through the reactor. In the IT mode, the difference between CO and CO_2 converted and methanol formed was estimated by the relation

$$err_{\text{IT}}=\frac{X_{\text{C}}(\dot{n}_{\text{CO}}+\dot{n}_{\text{CO}_2})_{\text{in}}-(\dot{n}_{\text{CH}_3\text{OH}})_{\text{out}}}{X_{\text{C}}(\dot{n}_{\text{CO}}+\dot{n}_{\text{CO}_2})_{\text{in}}} \tag{22}$$

The estimated difference was very low; the average value of err_{IT} for all IT experiments was 5%. In the HTG mode, the deviation was estimated by expression

$$err_{\text{HTG}}=\frac{\Delta tX_{\text{C}}[\dot{n}_{\text{CO}}+\dot{n}_{\text{CO}_2}]_{\text{in}}-\left(\Delta t\sum_{i=1}^{3}[\dot{n}_{\text{CH}_3\text{OH}}]_{\text{out},i}+\frac{\Delta m_{\text{liq}}x_{\text{liq,CH}_3\text{OH}}}{M_{\text{CH3OH}}}\right)}{\Delta tX_{\text{C}}[\dot{n}_{\text{CO}}+\dot{n}_{\text{CO}_2}]_{\text{in}}} \tag{23}$$

where the first term in the numerator represents the amount of CO and CO_2 that was converted in a time increment Δt, while the second term represents the amount of methanol released in Δt through exits $i=1,\ 2,\ 3$ (Figure 5). The third term accounts for the amount of methanol collected in the gas-liquid separator. However, the estimated average err_{HTG} for all experiments was found to be 4.5%.

The experimental total carbon conversion data are shown in Figures 7 and 8 for two different inlet gas compositions in both modes of operation, IT and HTG, respectively. It should be pointed out here that the data points are the true experimental values since the catalyst deactivation was accounted for in the model (see Eq. 16). As one can see, the measured total carbon conversion in the IT mode was always lower compared to that in the HTG mode, in spite of the fact that the catalyst was more deactivated during the HTG experiments which followed the IT experiments. The total carbon conversion in the IT mode asymptotically approached the equilibrium value at high contact times (m_{cat}/Q_v), which is considered to be expected performance. Conversely, the conversion in the HTG mode did not obey an asymptotic approach; there seemed to be no limit but complete carbon conversion, which was depended on the vapor pressure of

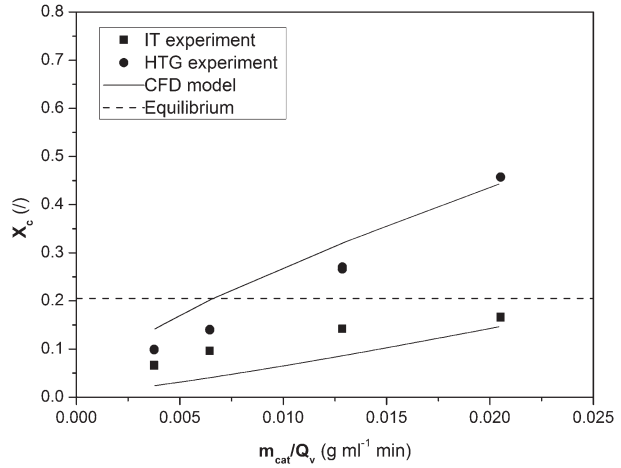

Figure 7. Total conversion of carbon *vs*. contact time in an isothermal (IT) and HTG experiment: $T_{cat} = 250°C$; $T_{cool} = 32°C$; $P = 25$ bar; $H_2/CO/CO_2 = 0.71/0.19/0.10$ (mol. %).

water and methanol in the gas phase at the cooled plate. In fact, at the highest contact time used, the conversion reached a more than three times higher value compared to the equilibrium (Figure 8). This increase was not that dramatic when the composition of the gaseous mixture at the reactor inlet was changed to lower hydrogen and higher carbon monoxide content (Figure 7).

Comparison of the total carbon conversion in the IT and HTG operation at different temperatures of the catalyst plate, that is, different temperature gradients, is depicted in Figure 9. Due to the thermodynamic constrains the IT operation yielded conversions almost independent of the catalyst temperature; the maximum that could be achieved was, indeed, the equilibrium one. With further temperature increase the conversion would start to decrease. Conversely, the HTG operation did not show limit in the conversion with respect to the catalyst plate temperature. The predicted and experimental data were found in a reasonable agreement but a slight underestimation of the former one.

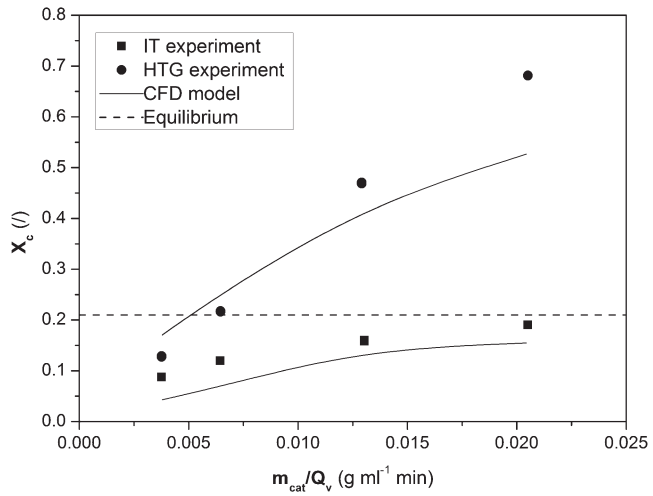

Figure 8. Total conversion of carbon *vs*. contact time in isothermal (IT) and HTG experiment: $T_{cat} = 250°C$; $T_{cool} = 32°C$; $P = 25$ bar; $H_2/CO/CO_2 = 0.78/0.12/0.10$ (mol. %).

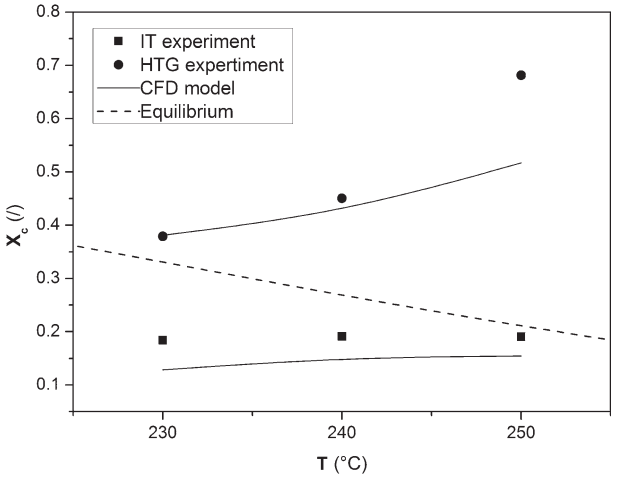

Figure 9. Total conversion of carbon *vs*. catalyst temperature in isothermal (IT) and HTG experiment: $m_{cat}/Q_V = 0.0205$ min g/mL; $T_{cool} = 32°C$; $P = 25$ bar; $H_2/CO/CO_2 = 0.78/0.12/0.10$ (mol. %).

Model Prediction and Limitations

To ensure uniform temperature distribution on the catalytic layer, and on the cooled surface in the HTG mode, the catalytic layer in width was 49 mm (24.5 mm in each side) less than the reactor niche. This part was planned to be filled with an appropriate insulating material but it was not possible to obtain it on the market. Therefore, in each side of the reactor niche, there was a part of the gas phase stream, which was not in contact with the catalytic layer and thus did not take part in the reactions directly, but mainly through the diffusion of CO, H_2, and CO_2 into the main reactant stream below the catalyst layer and the opposite diffusion of methanol and water into this part of the stream. Conversely, these parts of the gaseous stream were finally mixed with the stream flowing below the catalyst layer which resulted in its dilution that was recorded by GC in the exit stream. In other words, the experimentally measured conversions were positively lower than they would have been if the whole upper plate had been covered by the catalyst layer. As seen from Figures 7–9, the actual conversions for the experimental device used in this work are reasonably well predicted by the 3-D model used, which means that it correctly took into account the uncertainties caused by the two lateral streams.

Although the results predicted by the model show reasonable agreement with experimental data in general, one can examine the results for the case of erroneously measured temperature on the plates. Thus, a simulation for 5°C higher temperatures of the catalyst (i.e., using 255°C instead of 250) yields an increase of the total carbon conversion for about 8%. Since a 5°C lower temperature at the bottom (condensation) plate (25°C instead of 30) would only increase the conversion for 1.2%, the erroneous catalyst temperature seems to be the main source for a disagreement. The model sensitivity to heat transfer and flow rates for both modes of operation can best be seen on Figures 7–9.

Conversely, one would expect differences between predicted and experimental results because the rate parameters in equations (Eqs. 17–19) were evaluated at the conditions that were different from the conditions used in the HTG operation. Vanden Bussche and Froment[13] have proposed the

following equation for the methanol production from CO_2 hydrogenation (main methanol source)

$$r_{CH_3OH} \propto p_{CO} p_{H_2} \left(1 - \frac{1}{K} \frac{p_{H_2O} p_{CH_3OH}}{p_{H_2}^3 p_{CO_2}}\right) \beta^3 \quad (24)$$

where β is stands for the vacant active sites

$$\beta = \frac{1}{1 + (K_{H_2O}/K_8 K_9 K_{H_2})(p_{H_2O}/p_{H_2}) + \sqrt{K_{H_2} p_{H_2}} + K_{H_2O} p_{H_2O}} \quad (25)$$

From Eqs. 24 and 25, one can see that the reduction of partial pressures of water and methanol above the catalyst surface would not only directly increase the rate of methanol formation but would also dramatically increase it through the number of vacant active sites (by power of 3). Similar effects on the methanol production rate (with product removal) can be illustrated with other kinetic models for the methanol synthesis on Cu-based catalyst.[16,18] The above two reasons most probably contribute to higher experimentally measured rates compared to the predicted ones: this effect is positively more pronounced at higher hydrogen concentrations, when the methanol rates are higher (Figure 7). Partial pressures of water in the kinetic study[10] were above 0.05 bar, whereas simulation of the HTG operation showed that it was mostly below that value (see Figure 13). Thus, based on the comparison between experimental and predicted data one can conclude that the used rate parameters in equations (Eqs. 17–19) are not quite appropriate to be used in the extreme conditions (low water and methanol partial pressures) such as those in the HTG mode operation. Apart from the different operating conditions, the model's underestimation of the experimental values could partially be a consequence of the difference between the activity of the plate-catalyst prepared in this work and the catalyst used for the kinetic parameter estimation inside the CSTR reactor, described in the published kinetic study.[10] The variation can be attributed to the differences in the *in-situ* catalyst activation and pretreatment conditions inside the CSTR and the reactor described herein, which arise from the different mode of operation.

The calculated velocities at different longitudinal positions showed almost identical profiles in the IT mode but the velocity significantly decreased with y-coordinate in the HTG mode. This is due to much higher conversions found in the HTG mode and continuous condensation of methanol and water, which both reduced the volumetric flow rate of the reaction mixture. While the velocity profiles were symmetric in the IT mode, the profiles in the HTG mode exhibited asymmetry: the temperature decreased toward the condensation plate and consequently increased the gas phase density but decreased the viscosity, which resulted in a shift of the velocity profiles. The temperature profile with respect to the z-coordinate was found almost linear which is not surprising due to the laminar flow, and almost constant in the longitudinal direction.

Averaged cross-sectional values of the partial pressures of species participating in the methanol synthesis in HTG mode are shown in Figure 10. As expected, the methanol and water partial pressure slightly increased in the flow direction while the partial pressure of carbon dioxide decreased. Conversely, the partial pressure of carbon monoxide and hydrogen slightly increased along the length mainly on the account of continuous removal of methanol and water from

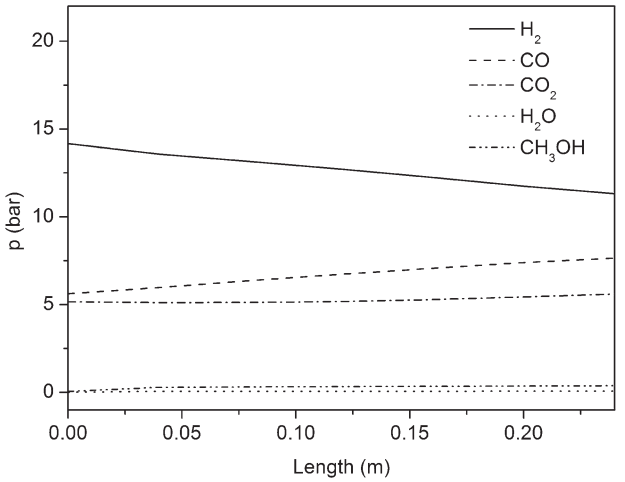

Figure 10. Average cross-sectional values of species partial pressures in HTG mode: $m_{cat}/Q_V = 0.0129$ min g/mL; $T_{cool} = 30$ °C; $P = 25$ bar; $H_2/CO/CO_2 = 0.78/0.12/0.10$ (mol. %).

the gas phase by condensation and very low consumption; in the case of carbon monoxide also on account of its formation through the RWGS reaction.

The simulated scalar field of carbon monoxide for the HTG mode within the slit domain is shown in Figure 11. As one can see, the partial pressure increases slightly with the longitudinal (y) direction, but not uniformly across the lateral (x) direction. In the vertical (z) direction, monoxide partial pressure starts increasing at the cool surface because of methanol and water condensation. The scalar field of carbon dioxide partial pressure shown in Figure 12 is even less uniform laterally: its high decrease is caused by the two reactions, which both consume carbon dioxide, the direct hydrogenation and RWGS reaction. One can also observe that due to its nonconsumption in the two lateral streams (without the catalyst layer above) the partial pressure keeps a higher value in those regions. Because of the high content of hydrogen in the reaction mixture, the partial pressure scalar field does not exhibit a dramatic change neither in the lateral nor longitudinal coordinate (not shown).

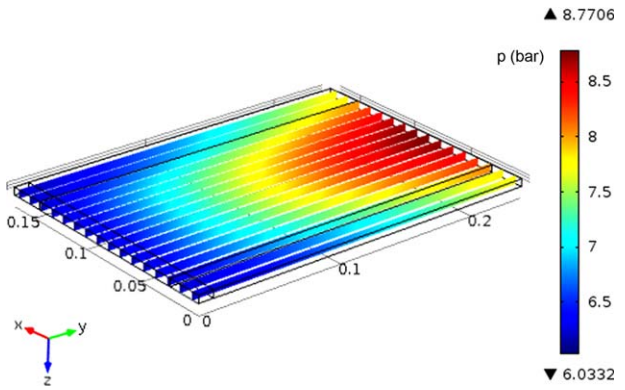

Figure 11. Calculated scalar fields of carbon monoxide partial pressure in HTG mode: $m_{cat}/Q_V = 0.0129$ min g/mL; $T_{cool} = 32$°C; $P = 25$ bar; $H_2/CO/CO_2 = 0.78/0.12/0.10$ (mol. %).

[Color figure can be viewed in the online issue, which is available at wileyonlinelibrary.com.]

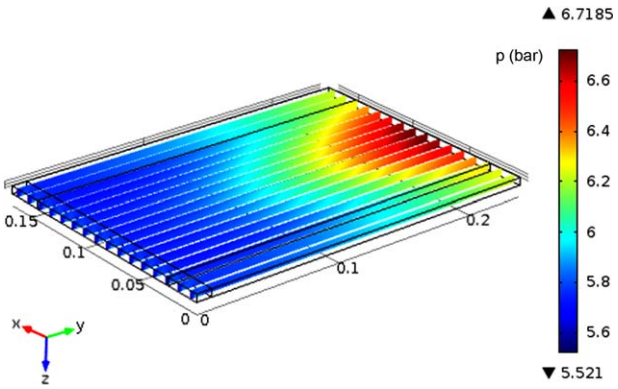

Figure 12. Calculated scalar fields of carbon dioxide partial pressure in HTG mode: $m_{cat}/Q_V = 0.0129$ min g/mL; $T_{cool} = 32°C$; $P = 25$ bar; $H_2/CO/CO_2 = 0.78/0.12/0.10$ (mol. %).

[Color figure can be viewed in the online issue, which is available at wileyonlinelibrary.com.]

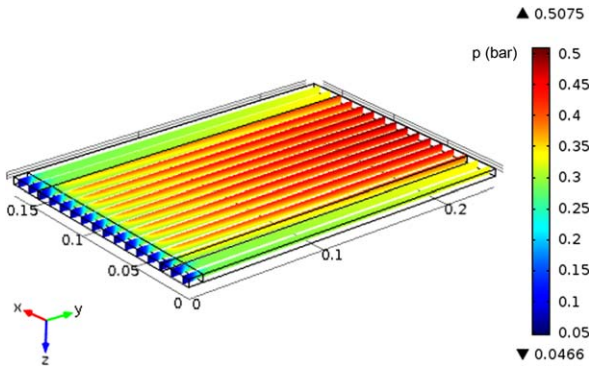

Figure 14. Calculated scalar fields of methanol partial pressure in HTG mode: $m_{cat}/Q_V = 0.0129$ min g/mL; $T_{cool} = 32°C$; $P = 25$ bar; $H_2/CO/CO_2 = 0.78/0.12/0.10$ (mol. %).

[Color figure can be viewed in the online issue, which is available at wileyonlinelibrary.com.]

The calculated scalar field of water partial pressure is depicted in Figure 13. As seen, water was already formed at the entrance into the slit but mostly at the catalyst surface and then its partial pressure gradually increased along the *y*- and *z*-directions. Nevertheless, the partial pressure was kept at a very low value while in the lateral streams its value was even lower, which alludes to the fact that the lateral diffusional process was relatively slow. Similar behavior was found with methanol (Figure 14). The partial pressure reached higher values at the catalyst layer surface down the second half of the niche. The gradients in *z*-direction were responsible for methanol and water flux toward the condensation plate and an increase of the rate of methanol formation.

The enhancement of methanol synthesis in the reactor was achieved by the continuous removal of the products from the reaction zone. For an optimal configuration, it is advantageous to position the top catalytic and the bottom condensation plate in close proximity, in order to provide a short diffusion path for the condensing products. A simulation was performed for $m_{cat}/Q_V = 0.0129$ min g/mL and the inlet gas composition $H_2/CO/CO_2 = 0.78/0.12/0.10$ for an increased distance between the top and bottom plate of 1 cm at the same linear velocity conditions (equal residence time). The results showed a decrease of the total carbon conversion from 53% (5-mm distance) to 39% (10-mm distance).

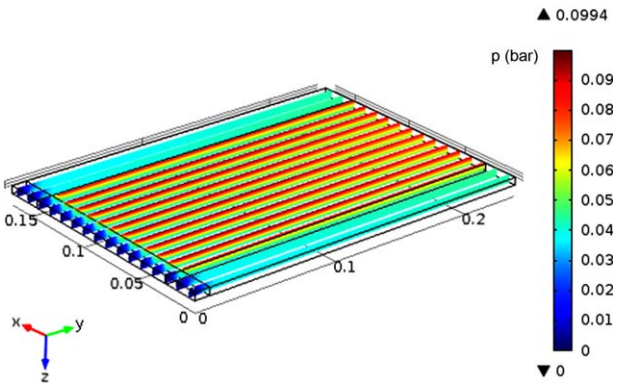

Figure 13. Calculated scalar fields of water partial pressure in HTG mode: $m_{cat}/Q_V = 0.0129$ min g/mL; $T_{cool} = 32°C$; $P = 25$ bar; $H_2/CO/CO_2 = 0.78/0.12/0.10$ (mol. %).

[Color figure can be viewed in the online issue, which is available at wileyonlinelibrary.com.]

The total mass flow fraction of the left and right bypass flow is 0.28 at the inlet, 0.31 at the middle of the channel, and 0.33 at the outlet of the reactor. For the case of methanol, convective flow in the in the direction of fluid flow, the convection represents approximately 99.9% of the total flow. Due to the laminar flow regime, the flow perpendicular to the flow direction is mainly governed by molecular diffusion. The convective flow in the direction of the depth represents only 2.4% of the total flow, while 97.6% is due to the diffusion. Diffusive flow in the direction of the width at the vertical plane between the catalyst and the bypass part of the channel represents 74% of the contribution to the total methanol flow. Reactor characteristics were evaluated through the calculation of the following relevant quantities. The reactor was operated at the volume hourly space velocities (VHSV) of 5000–27,000 h^{-1}. VHSV is defined as the total volumetric flow rate to the reactor at standard temperature and pressure, divided by the volume of the catalyst in the reactor. The volume averaged Péclet number inside the reactor, which is defined as the ratio of the rate of convection to the rate of diffusion, was less than 0.9 for all species. The small value indicates a significant contribution of diffusion to the transport of species, which is also a consequence of the low flow rate.

Conduction in the depth direction is the main mechanism of heat transfer due to the HTG inside the reactor, with 99.4% of the total heat exchanged in this manner. The average conductive heat flux in the direction of the depth was 3500 W/m^2. There is negligible amount of heat exchanged in the directions perpendicular to the depth, also on account of the low flow rate.

Conclusions

It was experimentally demonstrated that continuous removal of condensable products led to a considerable increase of conversion of a reversible catalytic reaction such as methanol synthesis: it was found to reach at least three times the equilibrium

conversion when the reaction was carried out in a 5-mm slit between hot plate-catalyst (250°C) and cool plate (32°C). With no temperature gradient between the plates, the conversion approached the equilibrium value. A 3-D-model reasonably well predicted the reaction behavior when both plates were at the same temperature. In the case of a high temperature difference between the plates, the predicted values were found slightly underestimated at high residence times when the reaction mixture was enriched with hydrogen. This alludes that the rate parameters evaluated by a conventional method may not be appropriate at conditions found in the HTG operation. A thin (95 μm) plate-catalyst prepared with a simple spraying method exhibited a very high stability even though it was applied on a relatively large surface of metal substrate.

Acknowledgment

The authors would like to thank Slovenian Research Agency (ARRS) for financing this work through a Grant P2–0152 and to Horjak Precise d.o.o. for the reactor fabrication.

Notation

$\hat{C}_p$ = specific heat capacity at constant pressure, J kg^{-1} K^{-1}
$\hat{D}_{jk}$ = multicomponent Fick diffusivities, m^2 s^{-1}
$\mathbf{d}_k$ = diffusional driving force for component k, m^{-1}
H = distance between catalytic layer and cool plate, m
$H_{\text{mix},j}$ = Henry's constant for component j in binary mixture, Pa
j_x = molar flux in x-direction, mol s^{-1} m^{-2}
j_y = molar flux in y-direction, mol s^{-1} m^{-2}
K_j = adsorption constant, bar^{-1} or bar$^{-1/2}$
$K^0_{p,i}$ = equilibrium constant for i-th reaction
$k'_{ps,i}$ = reaction rate constant for i-th reaction, mol s^{-1} bar^{-1} kg^{-1} or mol s^{-1} bar$^{-1/2}$ kg^{-1}
L = length of catalytic layer, m
m = mass, kg
M = molar mass, kg mol^{-1}
$\dot{m}$ = mass flow rate, kg s^{-1}
m_{cat} = catalyst mass, kg
N = total number of components, 5
$\dot{n}$ = molar flow rate, mol s^{-1}
p = partial pressure, Pa
P = total pressure, Pa
Q_v = volume flow rate, m^3 s^{-1}
R = gas constant, 8314 J mol^{-1} K^{-1}
r_i = reaction rate of i-th reaction, mol s^{-1} kg^{-1}
S_{cat} = geometric surface area of the catalyst, m^2
t = time, s
T = temperature, K
u = velocity components in y-direction, m s^{-1}
$\mathbf{u}$ = velocity vector, m s^{-1}
v = velocity components in z-direction, m s^{-1}
w = velocity components in x-direction, m s^{-1}
W = internal width of reactor, m
x = mole fraction, /
X_C = total carbon conversion, /

Greek letters

α = catalyst deactivation coefficient, /
λ = thermal conductivity, W m^{-1} K^{-1}
μ = viscosity, Pa s
$\nu_{j,i}$ = stoichiometric coefficient of component j in i-th reaction
ρ = density, kg m^{-3}
ω_j = mass fraction, /

Subscript

cat = catalyst
con = condensate
cool = bottom plate
eq = equilibrium
i = multipurpose index
in = inlet
j = j-th component
k = multipurpose index
liq = liquid
mix = mixture
out = outlet
ps = pseudo

Literature Cited

1. Amor HB, Halloin VL. Methanol synthesis in a multifunctional reactor. *Chem Eng Sci*. 1999;54:1419−1423.
2. Conant T, Karim A, Rogers S, Samms S, Randolph G, Datye A. Wall coating behavior of catalyst in non-poreus ceramic microstructures. *Chem Eng Sci*. 2006;61:5678−5685.
3. Conant T, Karim A, Datye A. Coating of steam reforming catalysts in non-porous multi-channeled microreactors. *Catal Today*. 2007; 125:11−15.
4. Curtis C F, Bird RB. Multicomponent diffusion. *Ind Eng Chem Res*. 1999;38:2515−2522.
5. Fukuhara C, Sasahara N, Igarashi A. Catalytic properties of nickel catalysts, for methanol decomposition, on aluminum plate prepared by electroless plating. *J Jpn Petrol Inst*. 1994;37:173−178.
6. Goldberger WM, Othmer DF. Kinetics of nickel carbonyl formation. *Ind Eng Chem Process Des Dev*. 1963;2:202−209.
7. Graaf GH, Stamhuis EJ, Beenackers AACM. Kinetics of low pressure methanol synthesis. *Chem Eng Sci*. 1988;43:3185−3195.
8. Halloin VL, Wajc SJ. A multifunctional catalytic reactor suitable for the exothermal synthesis of condensable products. *Chem Eng Sci*. 1994;49:4691–4698.
9. Haut B, Halloin V, Amor H. Development and analysis of a multifunctional reactor for equilibrium reactions: benzene hydrogenation and methanol synthesis. *Chem Eng Process*. 2004;43:979–986.
10. Perko D. Methanol formation enhancements in a multifunctional reactor, PhD thesis, University of Ljubljana, Ljubljana, SI, 2012.
11. Perko D, Levec J. Kinetic study of methanol synthesis over CuO/ZnO/Al_2O_3/V_2O_3 catalyst deposited on a stainless steel surface, *Ind Eng Chem Res*. 2012;51:710–718.
12. Phan XK, Bakhtiary HD, Myrstad R, Thormann J, Pfeifer P, Venvik HJ, Holmen A. Preparation and performance of a catalyst-coated foil microreactor for the methanol synthesis. *Ind Eng Chem Res*. 2010; 49:10934−10941.
13. Vanden Bussche KM, Froment GF. A steady-state kinetic model for methanol synthesis and the water gas shift reaction on a commercial Cu/ZnO/Al2O3 catalyst. *J Catal*. 1996;161:1−10.
14. Rozovskii AYa, Lin GI. Fundamentals of methanol synthesis and decomposition. *Top Catal*. 2003;22:137−150.
15. Shulgin I, Ruckenstein E. Henry's constant in mixed solvents from binary data. *Ind Eng Chem Res*. 2002;41:1689−1694.
16. Take T, Toshiaki Y, Tomura M, Kiyohara C, Ishino T, Kameyama H. Cu-Zn/Al2O3/Al-Plate catalyst for a methanol reformer. *J Chem Eng Jpn*. 2003;36:271−276.
17. Twigg MV, Spencer M S. Deactivation of copper metal catalysts for methanol decomposition, methanol steam reforming and methanol synthesis. *Top Catal*. 2003;22:191−203.
18. Van Bennekom JG, Venderbosch RH, Winkelman JGM, Wilbers E, Assink D, Lemmens KPJ, Heeres HJ. Methanol synthesis beyond chemical equilibrium. *Chem Eng Sci*. 2013;87:204−208.

Manuscript received Jun. 12, 2013, and revision received Oct. 16, 2013.